23

Image Resolution and Sensitivity Improvements of a Molecular Imaging Technique Based on Magnetic Nanoparticles

Yasutoshi Ishihara[1], Tsuyoshi Kuwabara[2] and Naoki Wadamori[2]
[1]*Meiji University,*
[2]*Nagaoka University of Technology*
Japan

1. Introduction

The enhanced permeation and retention (EPR) effect (Matsumura & Maeda, 1986) caused by the leakage of internally administered nanoparticles from blood vessels and their accumulation in cancerous tissues can be used to diagnose cancer. Gleich and Weizenecker proposed the magnetic particle imaging (MPI) approach (Gleich & Weizenecker, 2005), whereby the positions of these magnetic nanoparticles (MNPs) accumulated in cancerous tissue can be detected by applying a local alternating magnetic field from a source positioned outside the body. In basic MPI, the local magnetic field distribution is scanned to encode the spatial information, and the magnetization signal with odd-order harmonics is detected from MNPs inside a selected region when an alternating magnetic field is applied to the MNPs. Furthermore, a fast data acquisition method by scanning spatial data along with a Lissajous trajectory was proposed (Gleich et al., 2008; Knopp et al., 2009), and real time image-data acquisition was achieved (Weizenecker et al., 2009). However, interference from the magnetization signal generated from the MNPs outside the selected region degraded the image resolution and signal sensitivity (signal-to-noise ratio).

We proposed an image reconstruction method for reducing these interference signals mainly generated by even harmonics, and a correction method to suppress the interference signals (Kusayama & Ishihara, 2007; 2009; Ishihara & Kusayama, 2009). This was achieved by taking into account the difference between the saturated waveform of the magnetization signal detected from the MNPs outside the selected region and that detected from the MNPs inside the region. We performed numerical analyses to prove that the image resolution in the molecular imaging technique can be improved by using our proposed image reconstruction method, which is based on the abovementioned ideas. Furthermore, a fundamental system was constructed and the numerical analyses were experimentally validated using MNPs with diameters of 10–50 nm. The detection sensitivity and the resolution were improved by the use of methods in the case of locally distributed MNPs. However, a reconstructed image with the correct distribution of MNPs may not be obtained when the MNPs are distributed continuously. This is because the abovementioned proposed method acts as an intense high-pass filter against the reconstructed image (Ishihara & Kusayama, 2011).

These problems in MPI originate from the characteristics of the MNPs and the imperfect distribution of the magnetic field applied to the MNPs, as discussed later. Gleich and Weizenecker concentrated on the fact that the observational data overlapped the system function reflecting the characteristics of the MNP and the applied magnetic field distribution, and proposed an image reconstruction method for improving image quality (Gleich & Weizenecker, 2005). The abovementioned method involved performing an inverse matrix operation (such as singular value decomposition; SVD) (Weizenecker et al., 2007) or an iterative operation (algebraic reconstruction technique; ART) (Weizenecker et al., 2009) on the obtained data. However, when an image matrix becomes large, the use of this method to reconstruct images, which is based on a matrix operation, may result in the reconstructed images being underspecified.
Here, we propose a new image reconstruction method with higher image resolution and signal intensity. Our method is based on information regarding the correlation between the observed signal and a system function, and it does not use the inverse-matrix method.

2. Principle

2.1 Magnetization response generated by a MNP

The static magnetization (M) of a MNP exposed to a magnetic field is described well by the Langevin theory of paramagnetism, which is defined in equation (1).

$$M = M_s \left[\coth\left(\frac{m\mu_0 H}{k_B T} \right) - \frac{1}{\frac{m\mu_0 H}{k_B T}} \right] \tag{1}$$

where M_s is the saturation magnetization of a MNP, μ_0 is the magnetic permeability of vacuum, m is the magnetic moment of a particle $m = \pi D^3 M_s / 6$, H is the applied field, k_B is Boltzmann's constant, and T is the absolute temperature (Vekas et al., 2000).
A magnetization response with higher-order harmonics corresponding to the nonlinear magnetization properties of the MNP is generated when an alternating magnetic field is applied to a MNP (Fig. 1, [A]). However, such harmonics are not generated when a local static magnetic field that is strong enough to saturate the magnetization of the MNPs is applied (Fig. 1, [B]). The harmonics can be extracted by Fourier transformation of the detected signals; therefore, the positions of the MNPs can be identified and imaged by scanning the local distribution of a magnetic field which has approximately zero strength in the desired region (the field-free point, FFP) and is strong enough to saturate the magnetization in regions other than the FFP (Gleich & Weizenecker, 2005).

2.2 Fundamental MPI system

A fundamental MPI model is shown in Fig. 2 (a). A magnetic field distribution with very high field strength that surrounds the selected region, in contrast to having a first-order gradient at the center, is achieved by applying a DC current I_{DC} to two sets of Maxwell coil pairs. Thus, an FFP is formed at the center of these coils (Fig. 2 (b)). The position of this FFP is scanned by applying an offset DC current to each coil (Fig. 2 (c)). The MNPs generate a magnetization response because of the alternating magnetic field created by the AC current I_{AC} in the Maxwell coil pair consisting of the top and bottom coils. The response is detected as an electromotive force induced by the receiver coil according to Faraday's law.

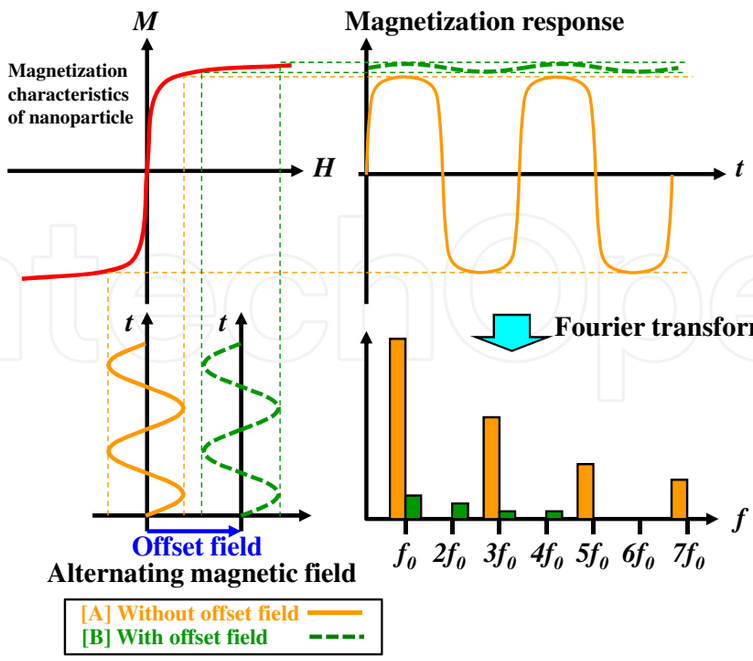

Fig. 1. Principle of MPI. MPI is based on the nonlinear magnetization properties of MNPs. When an alternating magnetic field with a frequency f_0 is applied to MNPs placed in a region where the static magnetic field strength is almost zero (FFP) [A], the MNPs generate a magnetization response with odd-order harmonics. In contrast, very few magnetization responses are detected from MNPs placed in a region where the magnetic field is strong enough to saturate their magnetization [B].

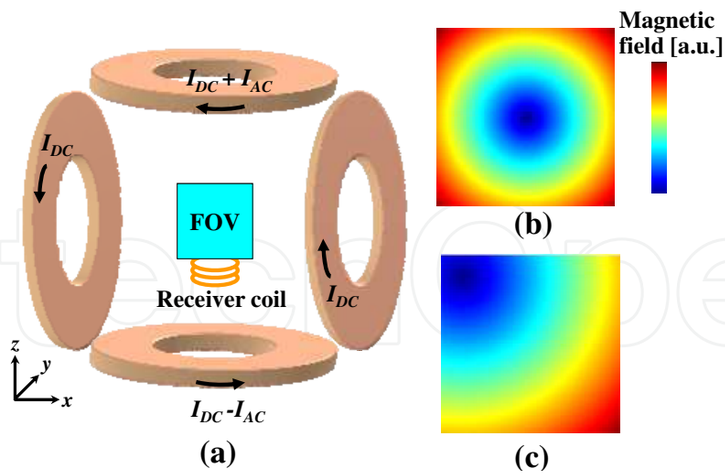

Fig. 2. Fundamental MPI model and generated magnetic field. Each Maxwell coil pair produces a magnetic field gradient along each axis. An FFP is formed at the center of the field of view (FOV), as shown in (b), when the DC currents applied to each coil are equal. The position of this FFP can be scanned by adjusting the ratio of currents applied to each coil (c). An alternating magnetization response is generated when an AC current is applied to the Maxwell coil pair consisting of the top and bottom coils. This response from the MNPs is recorded using a receiver coil.

2.3 Concept of image reconstruction by conventional method

As mentioned above, in MPI, image reconstruction is performed using the magnetization response waveform detected while scanning the FFP. In this approach, the shape of the FFP (the magnetic field distribution) applied to the MNPs has a significant influence on the resolution of the reconstructed image. For example, if the formed FFP is spatially localized by a steep magnetic field distribution as shown in Fig. 3 (a), image resolution comparable to the size of the FFP could be obtained. However, the local characteristics of the magnetic field distribution formed with the usual magnet are limited and imperfect (Fig. 3(b)). Moreover, the magnetizing properties (saturation characteristics) of the MNP also affect the spatial resolution. That is, the finite gradient of the magnetization curve limits the spatial resolution (Fig. 4). Under the influence of these two factors, an additional signal appears from the MNPs that are outside the boundary of the FFP, and interferes with the signal generated from the MNPs inside the FFP. This is shown in Fig. 5. When MNPs exist only in the center of the FOV, a signal is detected ideally only in the position of the desired FFP (*FFP-a,* shown in Fig. 5). However, when the gradient of the magnetic field distribution which forms the FFP is gently-sloping, or when the gradient of the magnetization curve of a MNP is finite, a signal is also detected from MNPs that are in a location other than the desired FFP (e. g., *FFP-b,* shown in Fig. 5).

Therefore, the conventional MPI image reconstruction method uses that the frequency spectrum of a magnetization response waveform would ideally consist only of odd harmonic components when the FFP is scanned at the point where the MNPs are located. Hence, when the FFP is in the two-dimensional plane (x-z plane) of $y = 0$ on Fig. 2, the signal strength in the reconstructed image is expressed by the following equation.

$$U(x,z) = \sum_{n=1}^{N_h} V\left[x, z, (2n+1)\right] \tag{2}$$

$U(x, z)$: reconstructed distribution in x-z plane

$V[x, z, n]$: n-th harmonic contained in the waveform at each FFP (x, z)

N_h: maximum harmonic order for reconstruction

However, because the amplitude is minute for the higher-order components, the information included in the higher-order components is not sufficiently utilized. Moreover, it is difficult to remove the interference caused by the imperfection of the two abovementioned factors using this method only, resulting in the appearance of a blur and an artifact in the reconstructed image.

In addition, from the MPI viewpoint, a larger MNP diameter is preferable according to the magnetization properties expressed in equation (1) (Yavuz et al., 2006), because a comparatively small alternating magnetic field is sufficient. On the other hand, because tens of nm is an effective distance for acquiring the EPR effect, a strong alternating magnetic field is required. This means that the influence of the abovementioned interference signal becomes large. Therefore, a method that successfully suppresses artifacts and improves detection sensitivity is indispensable.

3. Proposed methods

For typical MPI image-reconstruction, Weizenecker et al. (2009) proposed a method that performs an inverse-matrix operation on the obtained data by scanning the FFP along with a

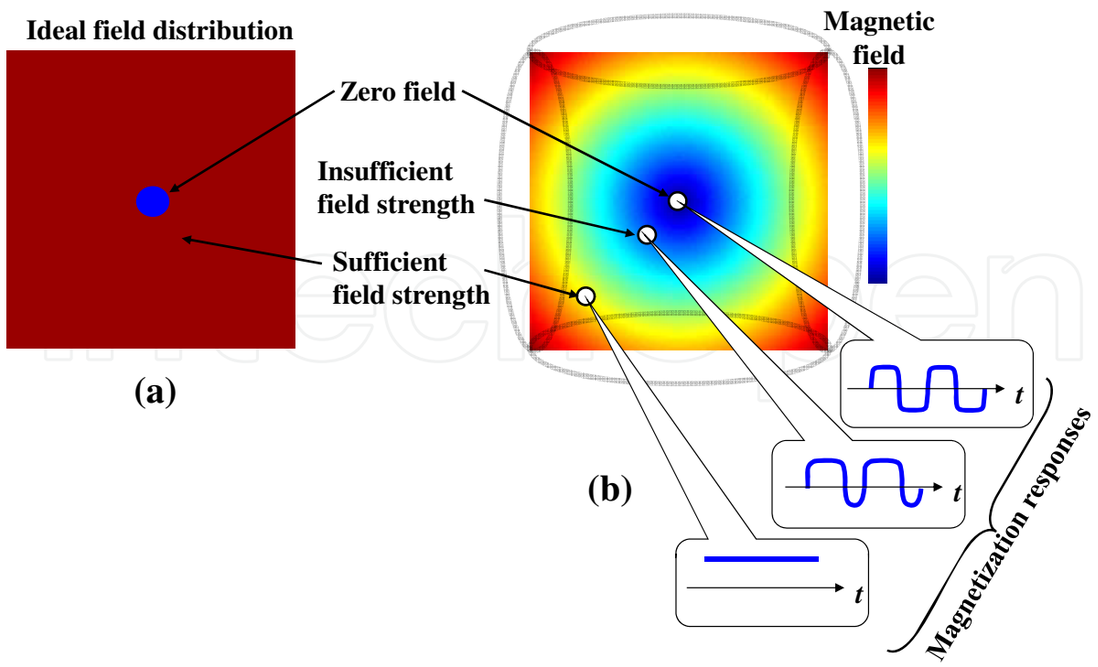

Fig. 3. Influence of FFP imperfection (magnetic field distribution). (a) Ideal FFP: The magnetic field strength is almost zero only in the area selected for acquiring a signal, in contrast to sufficient magnetization of MNP to reach saturation in other regions. (b) Actually formed FFP: the magnetic field distribution generated with Maxell coil pairs has a murky FPP boundary.

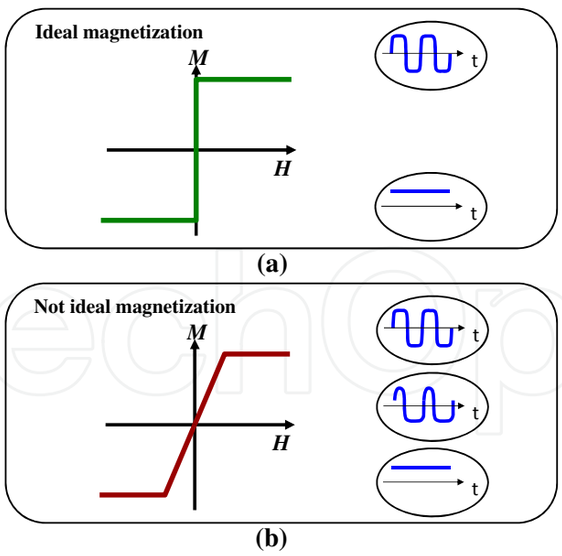

Fig. 4. Influence of imperfection in the MNP's magnetizing properties. (a) Ideal magnetization (saturation) property: when an alternating magnetic field is superimposed on an offset magnetic field, the AC component is not contained in the magnetization response of the MNP. (b) Not ideal magnetization (saturation) property: the AC component contained in the magnetization response of the MNP is affected by the offset magnetic field strength superimposed on an alternating magnetic field.

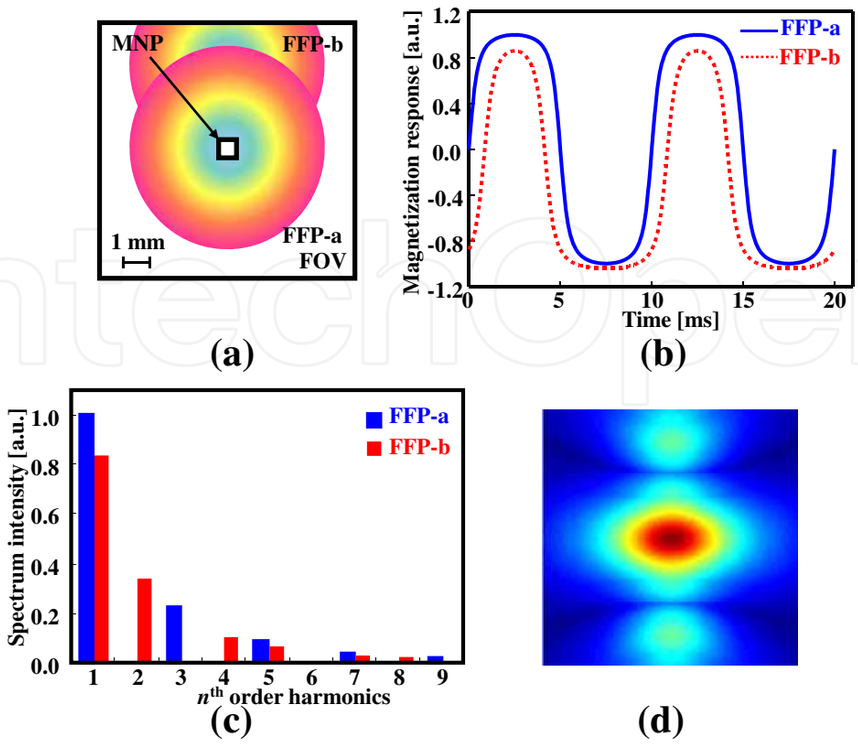

Fig. 5. Harmonic components detected at each FFP. A magnetization response composed of only odd harmonics is detected from the MNPs at the center of the FFP (FFP-a). Because the local magnetic field distribution that forms the FFP does not have a steep gradient, a magnetization response with even harmonics is also detected at a point where the FFP is at a certain distance from the MNPs (FFP-b).

Lissajous trajectory within the FOV, and delivered strong results. However, with this method, when the image size becomes large, a huge operation is needed, which raises concerns regarding the stability of the reconstructed image.
In this chapter, in order to reduce the image artifact and blurring, we first introduce the proposed method, and explain its efficiency and the problems it raises. Then, we propose an image reconstruction method that has excellent stability, image resolution, and detection sensitivity without performing inverse-matrix operations.

3.1 Adjusting the harmonic components

As explained in Fig. 5, in addition to the odd harmonics, considerable even harmonics are also detected in the signal when the FFP is set at a certain distance from a MNP owing to imperfections in the magnetic field distribution that forms the FFP. Although conventional MPI is reconstructed using only the odd harmonics based on equation (2), in the image reconstruction method proposed in this study, the odd harmonics are used, whereas the even harmonics are reduced, as defined in equation (3) (Kusayama & Ishihara, 2009). If the magnetic field distribution, which is formed as an FFP, and the magnetic characteristics of the MNP are known, the necessary components of the odd harmonics and the unnecessary component of the even harmonics can be determined. As a result, as shown in Fig. 6, the odd harmonics can be emphasized, and the even harmonics can be reduced.

$$U(x,z)=\sum_{n=1}^{N_h}\left\{V\left[x,z,(2n+1)\right]e^{\alpha(2n+1)}-V\left[x,z,(2n)\right]ke^{\beta(2n)}\right\} \quad (3)$$

$U(x, z)$: corrected distribution in x-z plane
$V[x, z, n]$: n-th harmonics contained in the waveform at each FFP (x, z)
N_h: maximum harmonic order for reconstruction
α, β: weighting factors for harmonics
k: arbitrary constants

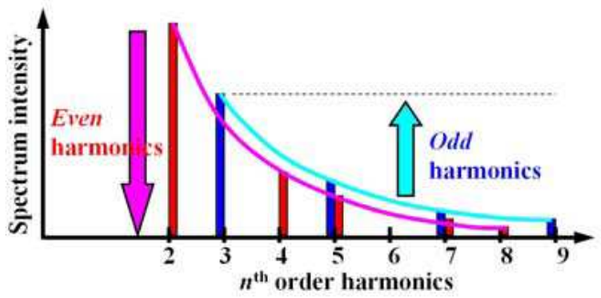

Fig. 6. Adjustment of harmonic components detected at each FFP. The odd harmonics were left unchanged and the even harmonics were reduced, in contrast to conventional image reconstruction methods.

3.2 Differentiating the waveforms obtained from inside and outside the FFP

Even if we use the method based on equation (3), the image resolution degrades because of the interference of the magnetization signals generated from several MNPs located outside the FFP boundary. For example, the signals generated from the MNPs located outside the FFP, as shown in Fig. 7 (a), may be composed of odd harmonics similar to those obtained from the MNPs placed inside the FFP. Because the effect of such interferences cannot be suppressed by the abovementioned procedure alone, the image artifact appears in the reconstructed image (Fig. 7 (d)), degrading the image resolution.

Here, a big difference is noticed when the waveforms generated from the MNPs inside the FFP region are compared with the interfering waveforms from outside the FFP region (Fig. 7 (b)). To distinguish between the interference signals, first, the offset component of the detected signal is corrected and normalization is performed. Second, the correlation between the corrected waveform and a waveform (system function) that is generated from a MNP at each FFP is evaluated. These processes are expressed in equation (4), and Fig. 8. Finally, this difference in waveforms is defined in terms of the correction factor, and suppression of unnecessary interference signals is attempted by multiplying their factors with the data determined from equation (3).

$$C_c=\left(1-N_s^{-1}\sum_{n=0}^{N_s-1}\left|\frac{w^i{}_n}{w^i{}_{\max}}-\frac{w_n-w_{mean}}{\left|w_{\max}-w_{mean}\right|}\right|\right)^{c_a} \quad (4)$$

N_s: number of sampling points
w_n, $w^i{}_n$: sampled interference and ideal waveform data
w_{max}, $w^i{}_{max}$: maximum value of each waveform
w_{mean}: mean value of interference waveform
c_a: arbitrary constant

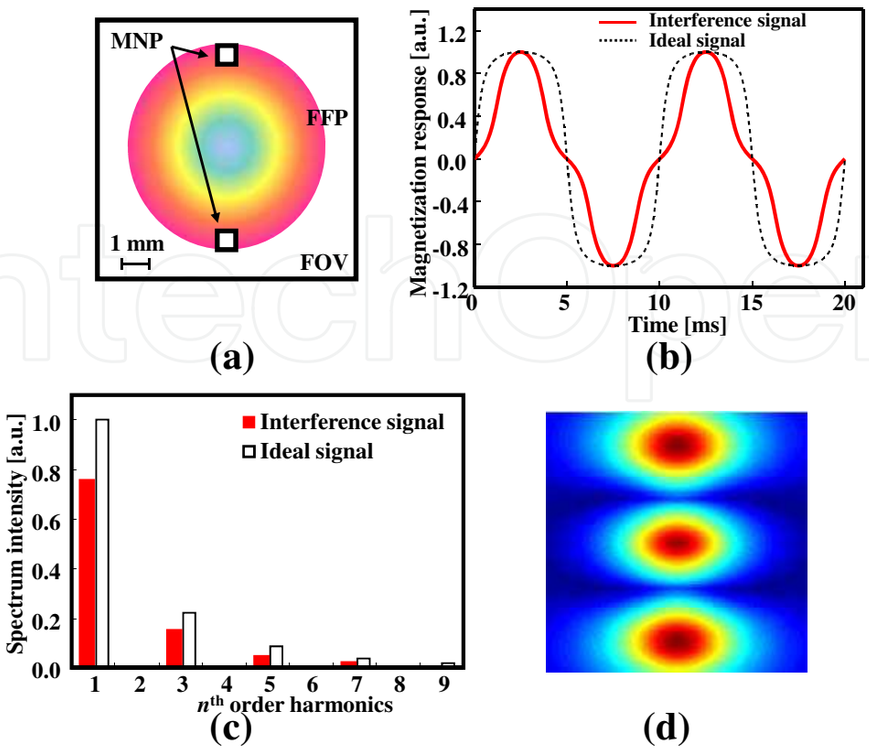

Fig. 7. Interference signal detected from regions outside the FFP. Because the magnetization response generated from the MNPs placed outside the FFP consists of odd harmonics at the FFP in the halfway point between MNPs, this interference cannot be eliminated by correction on the basis of the type of harmonics.

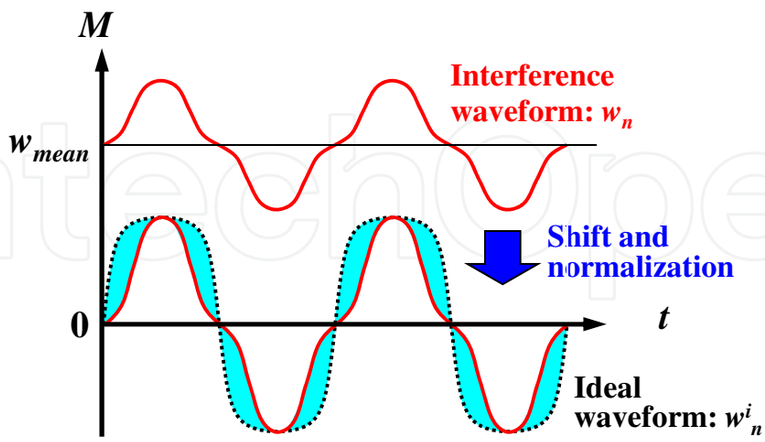

Fig. 8. Distinguishing the interference signal by using the correlation coefficient. In order to remove the interference of the magnetization signals, the following is performed: (1) correction of the offset component, (2) normalization of the waveform, (3) calculation of correlation coefficient, and (4) multiplication of correlation coefficient.

3.3 Correlating with the system function

The method proposed above is extremely effective in reducing blurring and artifacts in images, as will be shown later. However, this method emphasizes the signal from the isolated signal source that exists at the center of each FFP, and assumes that the signal generated from that circumference is an unnecessary interference. This is a problem when adjacent signal sources (MNPs) exist, as the intrinsic signal generated from these sources is recognized as an unnecessary interference to each other.

In order to overcome this unexpected effect, a method of reconstructing the exact spatial distribution of MNPs is proposed. Using the same method proposed by Weizenecker et al. (2009), the waveform generated from a MNP at each FFP is measured as a system function, but the correlation between this system function and a waveform generated by the unknown MNPs' distribution at each FFP is calculated without any inverse matrix operation. More specifically, the estimation of the MNPs' distribution is based on the correlation between the observed signal $S(x, z)$ from the unknown MNPs' distribution and the system function (*i.e.*, point-spread function) $G(i, j; x, z)$, which is a space-variant system determined by the interaction of the magnetic field and the MNPs' distribution. As shown in Fig. 9, this system function can be determined by measuring the waveforms at FFP points of (x, z) when a MNP is set at each point (i, j) within the FOV, and by connecting all these measured waveforms as one-dimensional data, which is sequentially arranged in an array of rows and columns (i, j). Consequently, the MNP distribution in the x-z plane is reconstructed using equation (5).

$$U(x,z) = \sum_{j=1}^{J}\sum_{i=1}^{I} S(x,z)G(i,j;x,z) \tag{5}$$

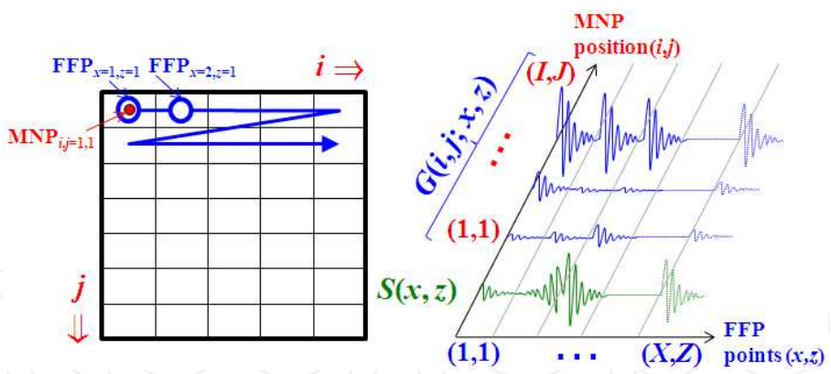

Fig. 9. Calculation of correlation coefficients: the system function $G(i, j; x, z)$ is defined as a space-variant system. It can be determined by measuring the waveforms at FFP points (x, z) when a MNP is set at each point (i, j) within the FOV. The MNP distribution is calculated by correlation with $S(x, z)$, which is the waveform measured by each FFP of (x, z) and arranged in a one-dimensional array.

4. Numerical simulation

4.1 Simulation methods

In order to examine the validity of the proposed method using the higher harmonic components appropriately, a numerical analysis using the system model shown in Fig. 2

was conducted. In this examination, two Maxell coil pairs (diameter: 50 mm, opposite distance: 50 mm) and a receiver coil (diameter: 16 mm, number of turns: 200) were used, and the FOV was set as 9 × 9 mm² with a matrix size of 64 × 32. A magnetic field distribution with a gradient magnetic field of about 5 T/m formed in the z direction at the MNPs with a particle diameter of 20 nm was applied as an FFP using this Maxell coil pair. In addition, an alternating magnetic field of 20 mT was applied in the same direction.

4.2 Simulation results

Figure 10 shows the reconstructed images of the MNP placed at the center of the FOV using the conventional method with equation (2) and the proposed method based on equation (3). The magnetic field was distributed over the region where the MNPs were positioned owing to the influence of the FFP formed as a result of the imperfection of the local magnetic field distribution. Therefore, because the alternating magnetic field was applied only in the z-direction, image blurring was observed particularly along the z-direction in the image reconstructed using the conventional method (Fig. 10(a)). On the other hand, such image blurring was reduced by suppressing the even harmonics on the basis of equation (3) and by using optimized parameters (N_h = 7, α = 0.19, β = 0.12, k = 1.39) (Fig. 10(b)).

Furthermore, it was confirmed that a drastic reduction in the image artifact compared to the conventional method could be achieved by using the proposed method shown in Fig. 11 by differentiating between the interference of the signal from the MNPs placed outside and inside the region on the basis of equation (4) using the optimized parameters (c_a = 10).

Although this proposed method enables us to improve image resolution by suppressing the interference signal due to the even harmonic components generated from the MNPs and also to improve the sensitivity by emphasizing the odd harmonic components, the outer part of the reconstructed image was weighted excessively, as in a high-pass-filter effect. For example, the perimeter region is emphasized when the MNPs indicate continuous distribution, as shown in Fig. 12 (a) while there are fewer blurring and artifacts compared with the conventional method shown in Figs. 10 and 11 when the MNPs are separated.

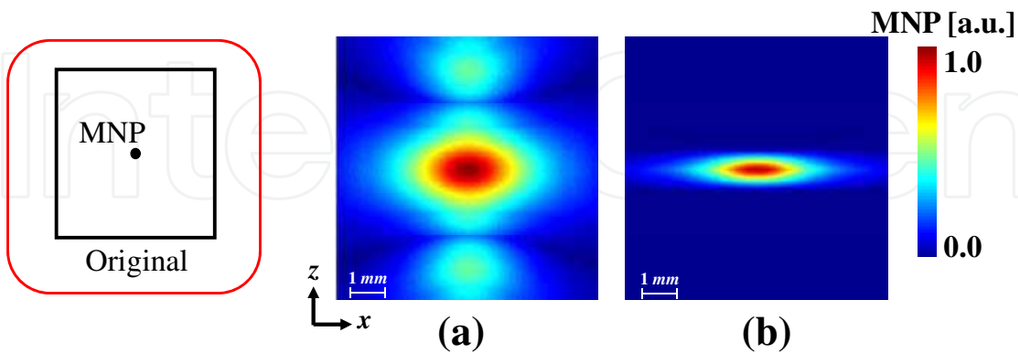

Fig. 10. Improvement of image resolution by adjusting the harmonic components based on equation (3). Overall image blurring due to the imperfection of the local magnetic field distribution formed as FFP is observed on the image reconstructed by the conventional method (a). The spread of the distribution along the z-direction was suppressed by using the proposed method with equation (3) (b).

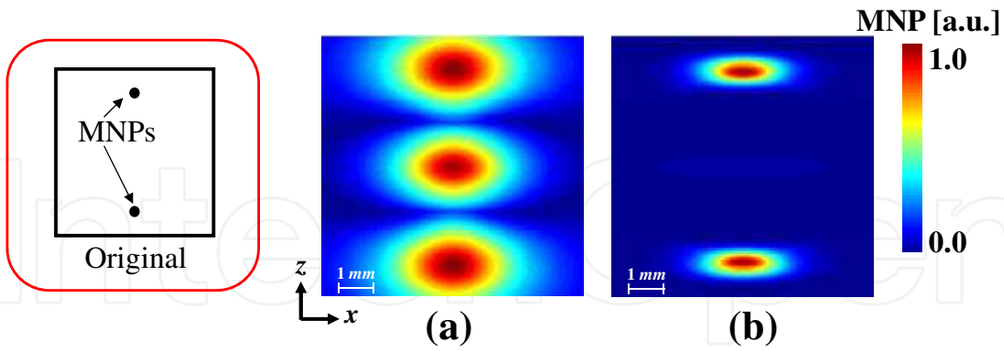

Fig. 11. Improvement of image resolution by suppressing the interference signals on the basis of equation (4). When using the conventional method, an image artifact was formed at the FFP between the nanoparticles placed symmetrically on either side of the FFP (a). With the proposed method, this image artifact was eliminated, and the spread of the field distribution in the *z*-direction was suppressed on the basis of equation (4) (b).

Consequently, the efficiency of the reconstruction method based on the newly proposed equation (5) was evaluated. Figure 13 illustrated the reconstructed results for the original image (Fig. 13(a)) using the conventional method (Fig. 13(b)), the method based on equations (3) and (4) (Fig. 13(c)), and the method based on equation (5) (Fig. 13(d)). With the conventional method, the reconstructed distribution was spread around the region where the MNPs were actually positioned, and an image artifact was observed. On the other hand, with the reconstruction method based on equation (5), although some image blurring is observed in the peripheral part of the image, a more exact reconstruction image with fewer artifacts is obtained, compared to other methods. Furthermore, it is confirmed from Fig. 14, which shows the profile of the central section of these images, that the sensitivity of this method based on equation (5) was high — about 20% compared with other methods.

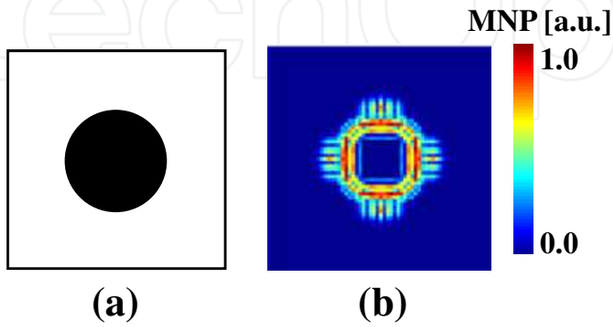

Fig. 12. The reconstruction result for a continuous distribution of MNP. The outer part of the reconstructed image is excessively emphasized, as in the effect of a high pass image filter.

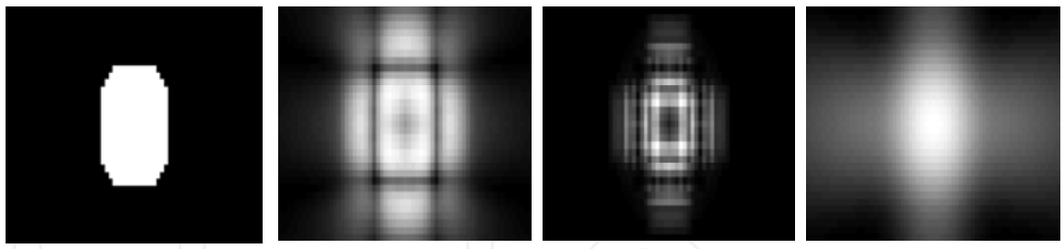

Fig. 13. Reconstruction results of each method. (a) Original image. (b) With the conventional method, significant image blurring and an artifact appear. (c) With the proposed method based on equations (3) and (4); although the image is less blurred, the edges are emphasized excessively. (d) With the proposed method based on equation (5); although the image is somewhat blurred, the original image is reconstructed more accurately than with the other methods.

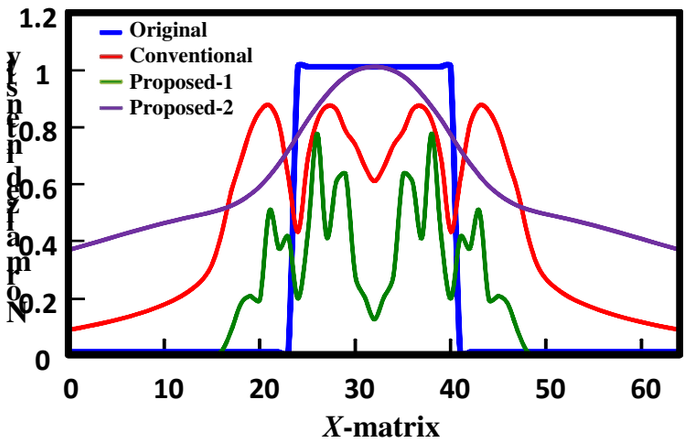

Fig. 14. Profile of a reconstructed image. The proposed method based on equation (5) reconstructs the MNP distribution more accurately than the other methods. In addition, this method has excellent sensitivity.

5. Experiment

5.1 Materials and methods

In order to confirm the validity of the proposed methods and numerical computation, the influence of the interference originating from the magnetization response waveform generated outside the target region was estimated by a fundamental experiment. The prototype Maxell coil pair (diameter: 180 mm, number of turns: 285 each, and opposite distance: 30–50 mm) (Toyojiki industry Co. Ltd., Niiza, Japan) used for the experiment is shown in Fig. 15.

5.1.1 Detecting magnetization response

When an alternating magnetic field was applied, the higher harmonic component contained in the magnetization response detected from the MNPs was evaluated, and the validity of the numerical analysis was confirmed. In this experiment, an alternating magnetic field with

an amplitude of about 90 mT was generated in the center of the coil by applying an alternating current (frequency of 35 Hz, and amplitude 10.6 A) in the same direction to each coil. As a measuring object, a 2.0-g dry particle of iron oxide (nominal diameter of 10 nm), which has polar surface properties (EMG1500, Ferrotec Corp., Chiba, Japan)) was enclosed in the container, as shown in Fig. 15 (b).
The magnetization response waveform generated from the MNPs at the center of the Maxwell pair coil was detected using a receiver coil (diameter: 35 mm, number of turns: 40) which surrounds the phantoms. Here, in order to reduce a nonlinear error, intrinsic to the system, which originates from imperfections in the power supplies and the Maxell coil pair, difference processing between the signals observed with and without the existence of the measuring object was carried out.

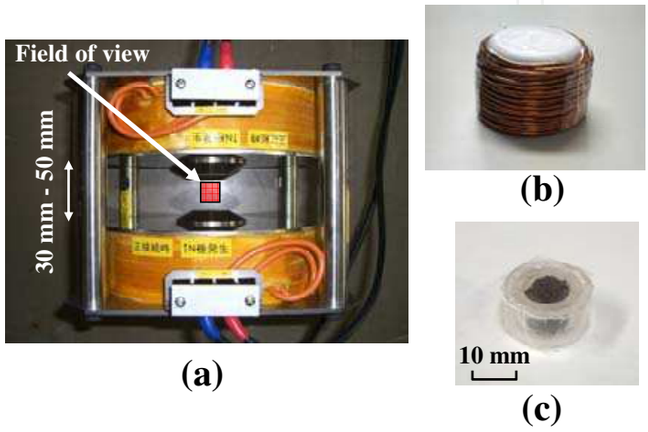

Fig. 15. Experimental modules for signal detection. A Maxwell coil pair (diameter: 180 mm, turns: 285 each, distance between coils: 30-50 mm) was used in the *z*-direction for generation of an FFP and an alternating magnetic field. The magnetization response from the dry particle of iron oxide enclosed within the container (c) was detected by a receiver coil (diameter: 35 mm, turns: 40) (b).

5.1.2 Differentiating the waveforms obtained from inside and outside of the FFP

Next, it was evaluated by the experiment that the interference of the magnetization response signal generated from MNPs outside an FFP can be decreased with the proposed method based on equations (3) and (4). In this experiment, an alternating magnetic field with an amplitude of about 20 mT was generated in the center of the coil by applying an alternating current (frequency of 80 Hz, and amplitude 4.7 A) in the same direction to each coil. At the same time, a direct current of 9.4 A was applied to each coil in the opposite direction and a gradient magnetic field of about 1.2 T/m was generated, and as a result, an FFP was generated around the center of the coil gap.
A 0.5-cc hydrophilic colloidal solution of superparamagnetic iron oxide (concentration about 500 mM/liter), which is coated with carboxydextran (Ferucarbotran, Fujifilm RI Pharma Co., Ltd., Tokyo, Japan), enclosed in the container shown in Fig. 16 (c) was used as a phantom. The magnetization response waveform generated from the MNPs at the center of the Maxwell coil pair was detected using a receiver coil (diameter: 35 mm, number of turns: 40) (Fig. 16 (a)) that surrounds the phantoms. In order to correspond to the numerical analysis (Fig. 11), the two phantoms were coaxially arranged, 20 mm apart, between the opposite coils (Fig. 16 (b)).

The FFP was set at the center between the coils, at an equal distance from the phantoms, and the magnetization response waveform generated from the phantoms was detected using the receiver coil (diameter: 23 mm, number of turns: 400) that surrounded the phantoms. The ideal waveforms (the system function) were determined by arranging a phantom at the center between the coils and measuring the signal, in order to calculate the correlation with the detected signal.

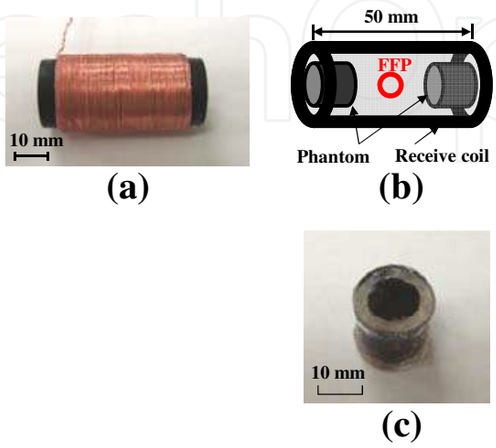

Fig. 16. Experimental modules for evaluation of the signal interference. The magnetization signal from the MNPs (MRI contrast agent: Ferucarbotran) (c), which are placed in two containers in order to reproduce the conditions of numerical analysis (b), was observed using a receiver coil (diameter: 23 mm, turns: 400) (a).

5.2 Experimental results

5.2.1 Detecting magnetization response

Figure 17 (a) shows the electromotive force induced by the receiver coil when applying the alternating magnetic field to the MNPs. By integrating over this electromotive force wave, the magnetization response waveform of the particles was obtained (Fig. 17 (b)) and is shown in Fig. 17 (c) with the result of the Fourier transform. These experimental results confirmed that the method of our numerical analysis is accurate.

5.2.2 Detecting magnetization response

The magnetization response waveform detected by the receiver coil and the ideal waveforms are shown in Fig. 18 (a). The influence of interference is reflected in the detected magnetization response waveform, and a similar wave shape to that shown in Fig. 7 was observed.

In order to confirm that the interference of the magnetization response waveform generated outside the FFP region can be suppressed by using the proposed method, the conventional method based on equation (2) and the proposed method based on equations (3) and (4) were applied to the magnetization response waveform obtained in the experiment. Here, the correction coefficients used in equations (3) and (4) were determined based on the characteristics of the ideal waveforms (N_h = 7, α = 0.10, β = 0.05, k = 1.22, c_a = 5.0).

The signal strength reconstructed by each method is shown in Fig. 18 (c). For the conventional method, the signal strength, which reflects the interference of the magnetization response waveform generated from outside the FFP, (which corresponds to

the interference signal detected at the center of the Maxwell coil pair) was about 79.0% of the ideal waveform signal. On the other hand, it was confirmed that this interference signal can be suppressed to about 9.0% by our proposed method based on equations (3) and (4).
The results of this fundamental experiment were well in agreement with the results of the numerical analysis, confirming the efficiency of the proposed methods and the computational process.

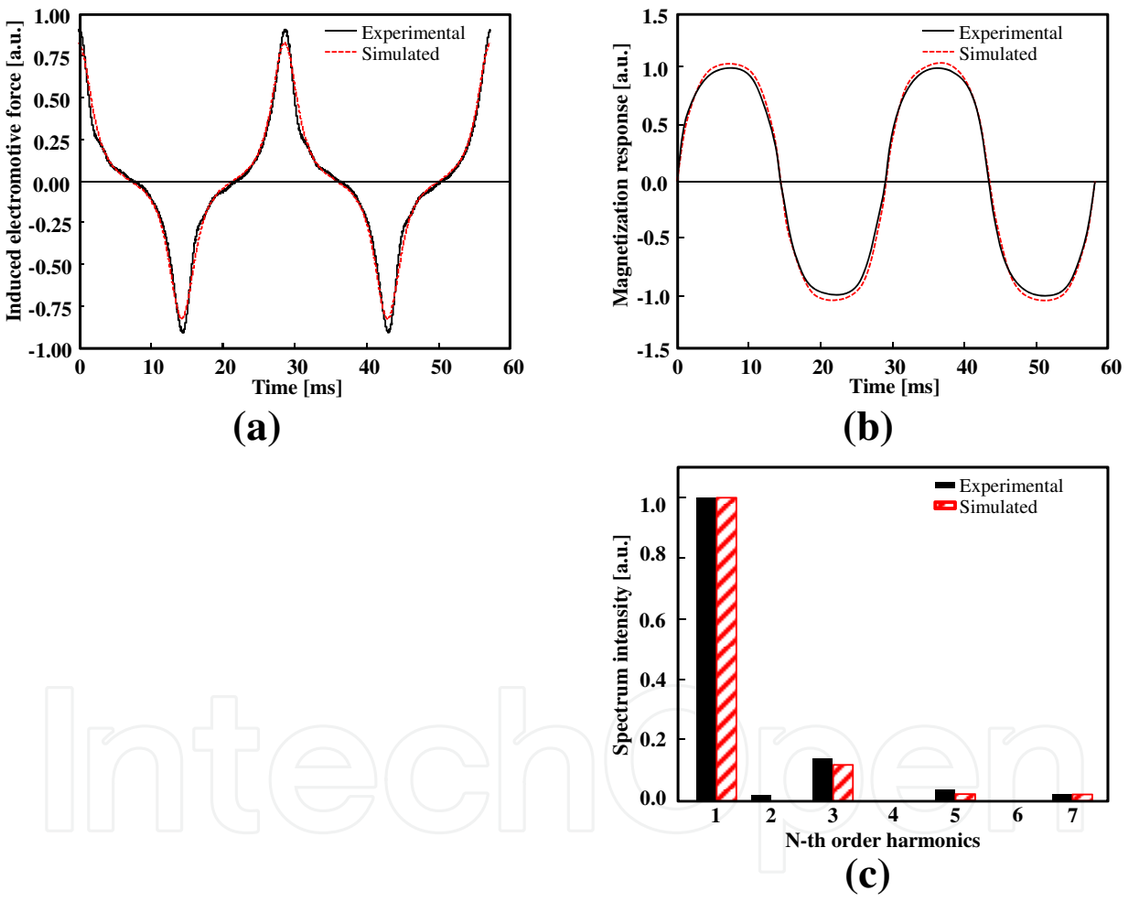

Fig. 17. Detected signal from MNPs. The signal from the MNPs is detected as electromotive force induced by the receiver coil (a). A magnetization response is obtained by integrating this signal (b), and the harmonics are computed by the Fourier transform of this response (c).

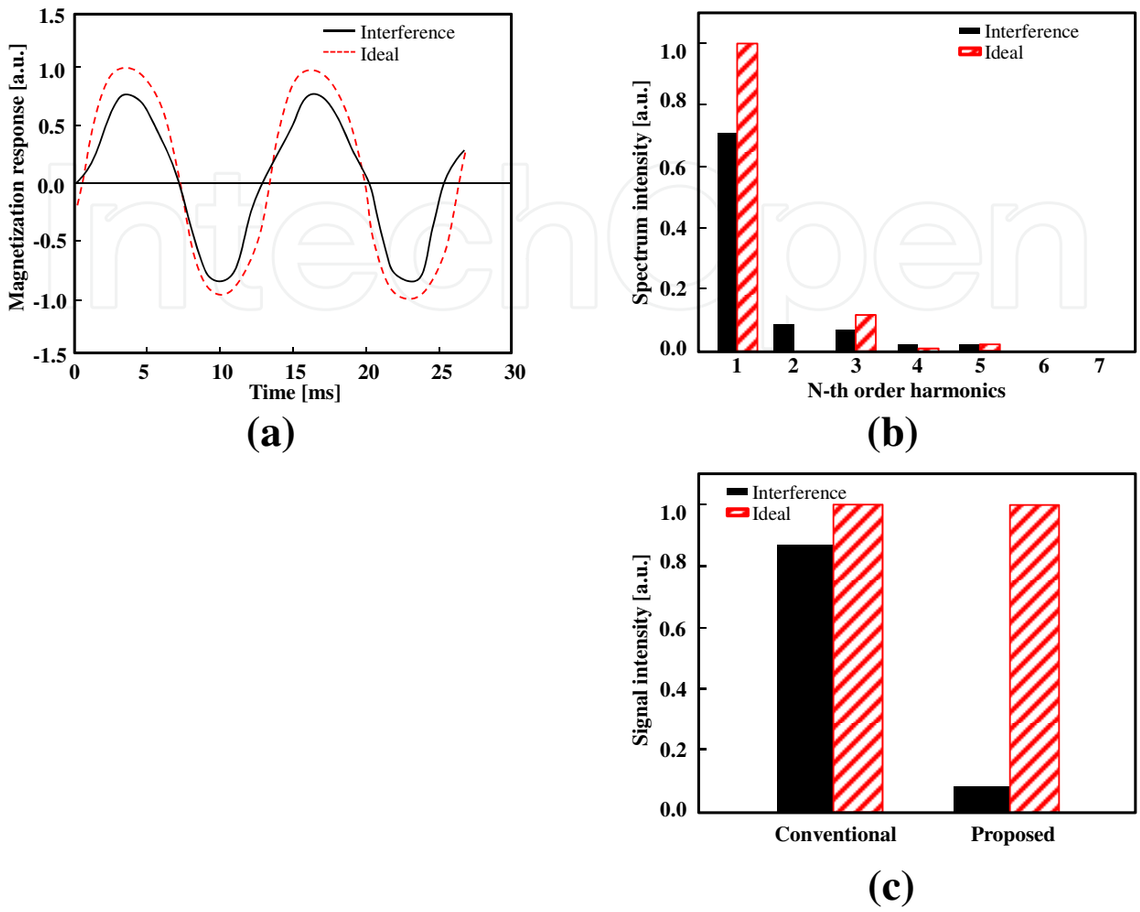

Fig. 18. Suppression effect of interference signal. It is confirmed that by using the proposed method, the interference signal detected from the center of the Maxwell coil (a) can be suppressed to less than 9.0% (c).

6. Conclusion

In MPI, interference of the magnetization signal generated from the MNPs outside the boundary of an FFP due to the nonlinear responses, results in degradation of the signal sensitivity. Although we proposed an image reconstruction method that suppresses the interference component while emphasizing the signal component using the property of the higher harmonic components generated from the MNPs, the perimeter of the reconstructed image was over-emphasized due to the high-pass-filter effect when using this method. We therefore proposed a new method based on the correlation information between the observed signal and a system function, and performed a numerical analysis. As a result, the image blurring was still visible, but we clearly showed that the detection sensitivity can be improved without the inverse-matrix operation used by the conventional image reconstruction method. In addition, although such proposed methods and numerical

analyses could be demonstrated by a basic experiment, the reconstruction of an image by means of a phantom experiment should be evaluated in the future.

7. Acknowledgements

This study was supported by a Grant–in–Aid for Scientific Research (B), 20300155, 2008 from the Japan Society for the Promotion of Science (JSPS).

8. References

Gleich, B. & Weizenecker, J. (2005). Tomographic imaging using the nonlinear response of magnetic particles. *Nature*, Vol. 435, No. 7046, Jun. 2005, 1214–1217, 0028-0836

Gleich, B.; Weizenecker, J., & Borgert, J. (2008). Experimental results on fast 2D-encoded magnetic particle imaging. *Phys. Med. Biol.*, Vol. 53, No. 6, Mar. 2008, N81–N84, 0031-9155

Ishihara, Y. & Kusayama, Y. (2009). Resolution improvement of the molecular imaging technique based on magnetic nanoparticles. *Proceedings of SPIE Medical Imaging 2009*, pp. 72584I.1–72584I.8, 978–0–8194–7509–1, Orlando, USA, Feb. 2009

Ishihara, Y. & Kusayama, Y. (2011). Sensitivity improvement of a molecular imaging technique based on magnetic nanoparticles. *Proceedings of SPIE Medical Imaging 2011*, Orlando, USA, Feb. 2011 (in press).

Knopp, T.; Biederer, S., Sattel, T., Weizenecker, J., Gleich. B, Borgert, J. & Buzug, T. M. (2009). Trajectory analysis for magnetic particle imaging. *Phys. Med. Biol.*, Vol. 54, No. 2, Jan. 2009, 385–397, 0031-9155

Kusayama, Y. & Ishihara, Y. (2007). A preliminary study on the molecular imaging device using magnetic nanoparticles. *Technical Report of IEICE*, MBE, Vol. 107, No. 218, Sep. 2007, 15–18, 0913-5685

Kusayama Y. & Ishihara, Y. (2009). High-resolution image reconstruction method on the molecular imaging using magnetic nanoparticles. *IEICE Trans. D*, Vol. J92–D, No. 9, Sep. 2009, 1653–1662, 1880-4535

Matsumura, Y. & Maeda, H. (1986). A new concept for macromolecular therapeutics in cancer chemotherapy: mechanism of tumoritropic accumulation of proteins and the antitumor agent smancs. *Cancer Res.*, Vol. 46, No. 12, Dec. 1986, 6387–6392, 0008-5472

Vekas, L.; Rasa, M. & Bica, D. (2000). Physical properties of magnetic fluids and nanoparticles from magnetic and magneto-rheological measurements. *J. Colloid Interface Sci.*, Vol. 231, No. 2, Nov. 2000, 247–254, 0021-9797

Weizenecker, J.; Borgert, J. & Gleich, B. (2007). A simulation study on the resolution and sensitivity of magnetic particle imaging. *Phys. Med. Biol.*, Vol. 52, No. 21, Nov. 2007, 6363–6374, 0031-9155

Weizenecker, J.; Gleich, B., Rahmer, J., Dahnke, H. & Borgert, J. (2009). Three-dimensional real-time *in vivo* magnetic particle imaging. *Phys. Med. Biol.*, Vol. 54, No. 5, Mar. 2009, L1–L10, 0031-9155

Yavuz, C. T.; Mayo, J. T., Yu, W. W., Prakash, A., Falkner, J. C., Yean, S., Cong, L., Shipley, H. J., Kan, A., Tomson, M., Natelson, D. & Colvin, V. L. (2006). Low-field magnetic separation of monodisperse Fe_3O_4 nanocrystals. *Science*, Vol. 314, No. 5801, Nov. 2006, 964–967, 0036-8075

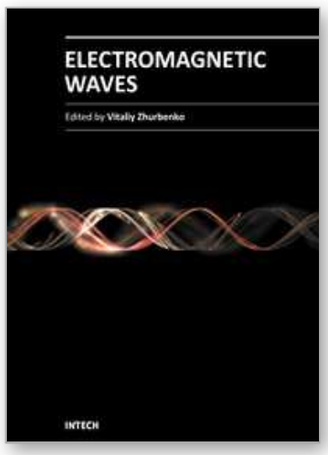

Electromagnetic Waves

Edited by Prof. Vitaliy Zhurbenko

ISBN 978-953-307-304-0
Hard cover, 510 pages
Publisher InTech
Published online 21, June, 2011
Published in print edition June, 2011

This book is dedicated to various aspects of electromagnetic wave theory and its applications in science and technology. The covered topics include the fundamental physics of electromagnetic waves, theory of electromagnetic wave propagation and scattering, methods of computational analysis, material characterization, electromagnetic properties of plasma, analysis and applications of periodic structures and waveguide components, and finally, the biological effects and medical applications of electromagnetic fields.

InTech Europe
University Campus STeP Ri
Slavka Krautzeka 83/A
51000 Rijeka, Croatia
Phone: +385 (51) 770 447
Fax: +385 (51) 686 166
www.intechopen.com

InTech China
Unit 405, Office Block, Hotel Equatorial Shanghai
No.65, Yan An Road (West), Shanghai, 200040, China
中国上海市延安西路65号上海国际贵都大饭店办公楼405单元
Phone: +86-21-62489820
Fax: +86-21-62489821

IntechOpen